ORNL-5857

ornl

OAK RIDGE NATIONAL LABORATORY

UNION CARBIDE

Weld-Metal Grain Structure and Mechanical Properties of Iridium Alloy DOP-26

C. T. Liu
S. A. David

METALS and CERAMICS
ENERGY
RESEARCH
DEVELOPMENT
OAK RIDGE NATIONAL LABORATORY

OPERATED BY
UNION CARBIDE CORPORATION
FOR THE UNITED STATES
DEPARTMENT OF ENERGY

Printed in the United States of America. Available from
National Technical Information Service
U.S. Department of Commerce
5285 Port Royal Road, Springfield, Virginia 22161
NTIS price codes—Printed Copy: A03 Microfiche A01

ORNL-5857
Distribution
Category UC-23

METALS AND CERAMICS DIVISION

ORNL--5857

DE82 019899

WELD-METAL GRAIN STRUCTURE AND MECHANICAL PROPERTIES OF IRIDIUM ALLOY DOP-26

C. T. Liu and S. A. David

Date Published - August 1982

NOTICE: This document contains information of a preliminary nature. It is subject to revision or correction and therefore does not represent a final report.

Prepared by
OAK RIDGE NATIONAL LABORATORY
Oak Ridge, Tennessee 37830
operated by
UNION CARBIDE CORPORATION
for the
DEPARTMENT OF ENERGY
Under Contract No. W-7405-eng-26

Blank Page

CONTENTS

WELD METAL GRAIN STRUCTURE AND MECHANICAL PROPERTIES OF IRIDIUM ALLOY DOP-26*

C. T. Liu and S. A. David

ABSTRACT

Weld metal grain structure and mechanical properties of the Ir–0.3% W alloy (DOP-26) doped with 60 ppm Th and 50 ppm Al have been investigated by use of a gas tungsten arc (GTA) welding process. The fusion zone grain structure is strongly influenced by heat input and puddle shape and therefore by the bead width. With increasing bead width from 2.5 to 3.7 mm, the grains in the fusion zone show a sharp change in growth direction near the centerline region and develop a fine columnar structure with grains growing parallel to the welding direction. Mechanical properties of the welds and base metal were characterized by tensile and impact tests from 650 to 1150°C. The ductility and fracture behavior of DOP-26 welds are sensitive to weld bead width, postweld heat treatment, and weld-test orientation. The ductility of the welded specimens increases with increasing test temperature and decreasing weld bead width. The transverse weld specimen with a wide-bead width (3.7 mm) has the lowest impact ductility, and the longitudinal weld with a narrow-bead width (2.5 mm) has the highest elongation at all the test temperatures. The impact ductility of the transverse weld specimen with the narrow-bead width falls between the limits. All the results are discussed in terms of the fusion zone grain structure and fracture path of the welds.

INTRODUCTION

Iridium is an fcc metal having very unusual mechanical properties. Iridium metal has an exceptionally high elastic modulus,[1] critical resolved shear stress,[2–4] and work hardening rate.[2–4] It exhibits a cleavage-type fracture on tensile tests, which is not observed in other

*Research sponsored by the Office of Coordination and Special Projects, Department of Energy, under contract W-7405-eng-26 with the Union Carbide Corporation.

fcc metals.[5] The cleavage fracture has been observed in iridium at temperatures as high as 1000°C.[6,7] Polycrystalline iridium shows grain boundary fracture with limited ductility in tensile tests below 800°C at conventional speed (10^{-4} m/s) or in impact tests to at least 1500°C at high velocities (>10 m/s).[6,8] Recent studies of intergranularly fractured surfaces with Auger electron spectroscopy showed no evidence of impurity segregation that might be responsible for the grain boundary failure of iridium and its alloys.[7,9]

Currently, Ir—0.3% W alloys doped with 30 to 60 ppm Th are used as postimpact containment material for radioactive fuel in thermoelectric generators that provide stable electrical power for a variety of outer planetary missions.[10] Iridium alloys were chosen for this application because of their high melting point (2450°C), good high-temperature strength, oxidation resistance, and compatibility with oxide fuel forms and insulation materials. Tungsten at a level of 0.3% has been alloyed to improve the fabricability of unalloyed iridium. Thorium is added as a grain boundary,[10,11] segregating strongly to the grain boundaries and inhibiting intergranular fracture during high-temperature, high-velocity reentry impact from space. Thorium additions also react with iridium to form $ThIr_5$ precipitates, which pin the grain boundaries and retard the grain growth during long-term service at the 1200 to 1400°C operating temperatures.

Weldability studies have shown that iridium alloys containing less than 100 ppm Th can be successfully welded by a gas tungsten arc (GTA) process without hot cracking.[12] However, the mechanical properties of these iridium alloys depend strongly on grain structure,[8,11] and development of coarse unfavorable microstructures in GTA welds may severely reduce the ductility and impact strength of a welded joint. To overcome this problem we judiciously selected weld process parameters to control heat input and solidification rate and thereby solidification structure.[12—14] An Ir—0.3% W alloy doped with 60 ppm Th and 50 ppm Al, designated as DOP-26 alloy, was welded by a GTA process under controlled conditions, and the mechanical properties of the welds were characterized by tensile and impact tests from 650 to 1150°C. The results thus obtained

are also compared with the base-metal properties. Emphasis is on correlation of the mechanical properties with fusion zone grain structure, heat treatment, and fracture path.

EXPERIMENTAL PROCEDURES

The DOP-26 alloy used in this study was arc melted and drop cast in a chilled copper mold. The ingots were clad in molybdenum and hot rolled to 0.89 mm at 1000 to 1200°C. Following hot rolling, the sheets were ground to a final thickness of 0.64 mm (0.025 in.) and cleaned in a potassium cyanide solution to remove impurities or oxide scales from the surface. Table 1 lists the chemical composition of the alloy as determined by spark source mass spectroscopy (SSMS), fusion, and carbon analyses.

Autogeneous bead-on-plate and butt welds were made on 0.64-mm-thick samples in a glove box containing 75% He–25% Ar. To provide a fully recrystallized grain structure, all samples were vacuum-annealed for 1 h at 1500°C. The fusion zone grain structure was controlled by transverse arc oscillation, heat input, and postweld heat treatment. On the basis of

Table 1. Typical chemical composition of Ir–0.3% W alloy determined by spark source mass spectroscopy, fusion, and carbon analyses

Element	Concentration (ppm)	Element	Concentration (ppm)
Al	42	Ru	8
B	<0.1	Si	6
Cr	3	Ta	8
Cu	5	Th	52
Fe	10	W	3400
Mo	30	C	8
Ni	2	H	2
P	<0.1	N	1
Pt	<10	O	10
Rh	5		

early studies involving a range of frequency and welding speed,[12–14] we selected and used a transverse arc oscillation frequency of 375 cycles/min and a welding speed of 76 cm/min. The surface bead width of the welds was governed by the power input and chilling conditions. Welds with two surface bead widths, namely 3.7 mm (wide bead width) and 2.5 mm (narrow bead width), were used.

The samples were subjected to postweld heat treatment from 1290 to 1800°C in vacuum. Various sections of the joints in the as-welded and heat-treated conditions were prepared for metallographic examination by standard techniques. The samples were etched electrolytically in a solution of 400 mL H_2O, 100 mL HCl, and 50 g NaCl in a stainless steel container with an ac power supply.

Tensile testing was done on an Instron machine at a crosshead speed of 2.5 mm/min. Tensile specimens having a gage section 3.18 mm wide and 12.7 mm long were prepared by an electric discharge machine, with edges ground to remove burning debris. Figure 1 shows the longitudinal and transverse weld specimens used. To perform the tensile test at 650°C,

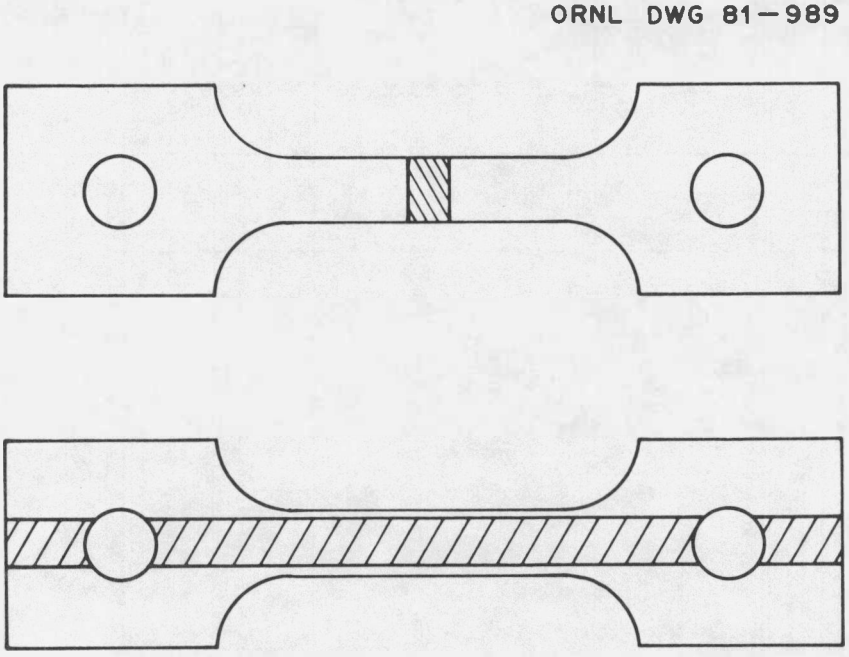

Fig. 1. Configuration of welded specimens. (a) Transverse weld specimen. (b) Longitudinal weld specimen.

a water-cooled quartz-tube vacuum system was attached to the Instron machine, and specimens were heated inductively inside a tantalum susceptor. The load-time curves were used to generate the stress-strain data. Fracture surfaces of selected specimens were examined by a JSM-V3 scanning electron microscope (SEM) operated at 25 kV.

Uniaxial impact tests were performed in an environmentally controlled impact chamber with a 7.62-cm-diam gas gun to accelerate the projectile (bullet) at a velocity of 61 m/s (200 fps). Figure 2 shows the arrangement of tensile specimens for impact testing. The specimens were loaded between two molybdenum alloy (TZM) pull rods and an end plate and were heated by radiation from an inductively heated tantalum susceptor; the test temperature was monitored by a Pt vs Pt—10% Rh thermocouple centrally located on the specimen. When the specimens reached the desired temperature, the air-driven projectile was fired at known velocity to break them. The impact elongation and fracture mode were determined by examining the fractured specimens.

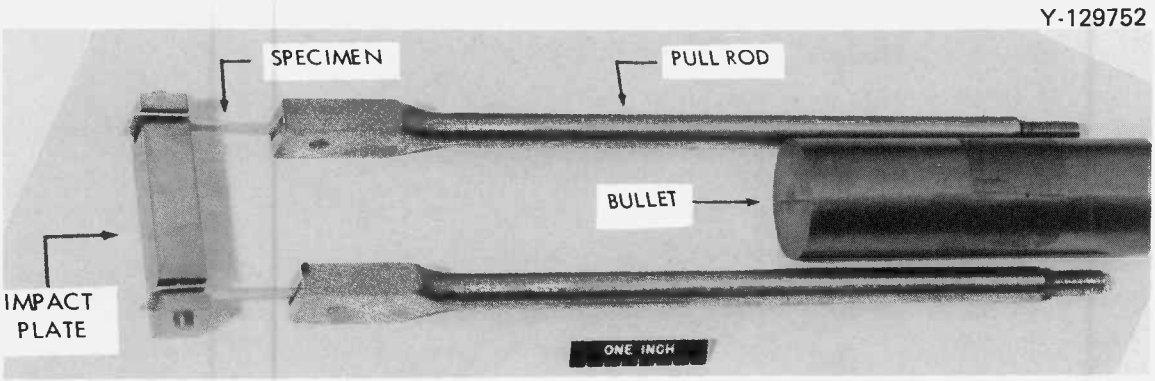

Fig. 2. Arrangement of tensile specimens for uniaxial impact test.

RESULTS

Microstructure of Welds

Metallographic examination revealed that the fusion zone grain structure of DOP-26 GTA welds depends strongly on heat input and puddle shape and therefore on the bead width. Figure 3 shows the microstructure typical of a butt weld with a narrow-bead (2.5-mm) width. The grains in the fusion zone are fine and appear to nucleate on the partially melted base

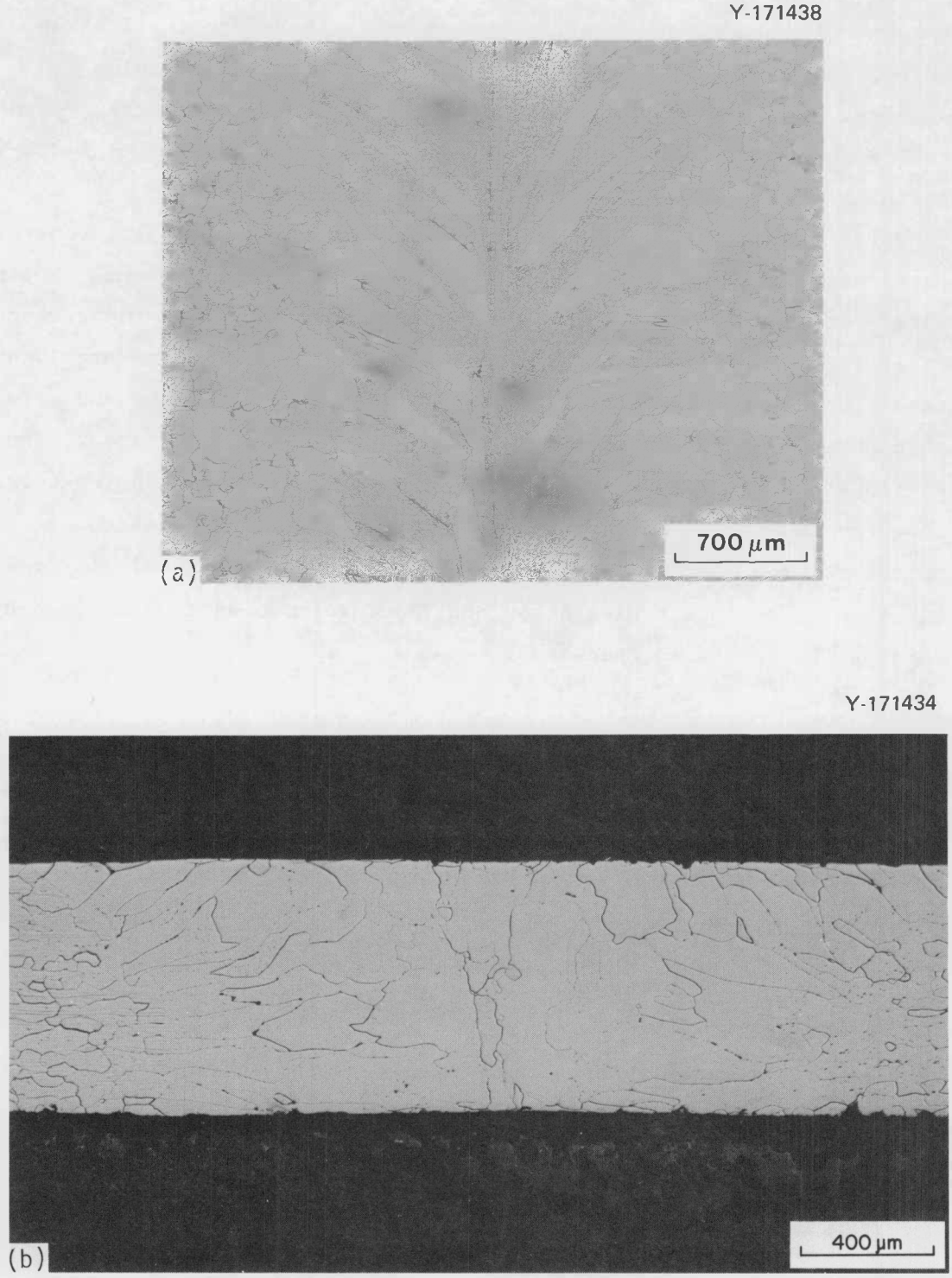

Fig. 3. Fusion zone microstructure of a DOP-26 weld with a narrow-bead (2.5-mm) width; no postweld heat treatment. (a) Top surface. (b) Transverse section.

metal grains and to grow continuously, with most of the grains exhibiting a considerable curvature. Figure 4 shows the microstructure typical of a butt weld with a wide-bead (3.7 mm) width. The grains in this weld appear to nucleate on the partially melted base metal grains and to continue growing almost normal to the welding direction until reaching the centerline region. In the centerline region, the grains show a sharp change in growth direction and develop a fine columnar structure with grains growing parallel to the welding direction. The microstructure of the transverse section of the weld revealed a narrow band of fine-grain structure along the centerline of the weld [Fig. 4(b)]. Note that neither weld shows a well-defined heat-affected-zone.

The microstructure of the wide and narrow welds was also examined after postweld heat treatments. Figure 5 shows the fusion zone structure of the narrow weld annealed 1 h at 1500°C. Comparison of Figs. 3 and 5 indicates no apparent change in structure by the heat treatment. The solidification substructure within grains of the fusion zone can be revealed at high magnification, as shown in Fig. 6. The substructure is predominantly cellular dendritic with a cell size of about 5 μm. The welds show considerable coarsening in the fusion zone grain structure after a severe heat treatment of 1 h at 1650°C* plus 2 min at 1800°C.†

Tensile Properties

Table 2 summarizes the tensile properties of DOP-26 GTA welds tested at 650°C. Some of these data points represent an average of two tests. The base metal is ductile with a tensile elongation exceeding 30%. In comparison, the welded specimens show higher yield strength but much lower ductility. The tensile ductility of the welds depends strongly on surface bead width, weld-test orientation, and postweld heat treatment. The tensile elongation is significantly higher for the narrow-bead weld than for the wide-bead weld. Both types of welds show a remarkable increase in ductility and a decrease in yield strength after a postweld treatment of

*To simulate the grain growth of DOP-26 alloy during six months aging at 1330°C in space power systems.

†To simulate the dynamic heating during reentry of space power systems.

Y-171441

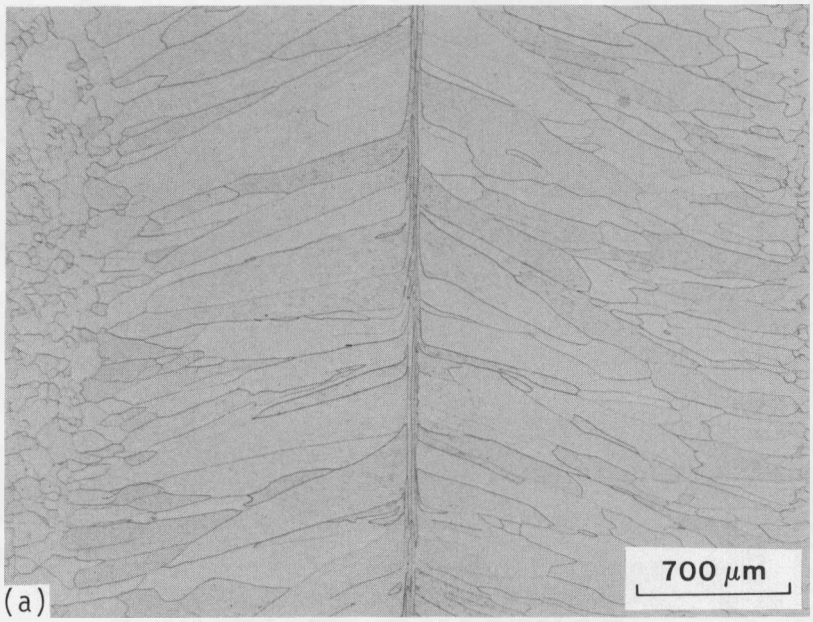

Y-171437

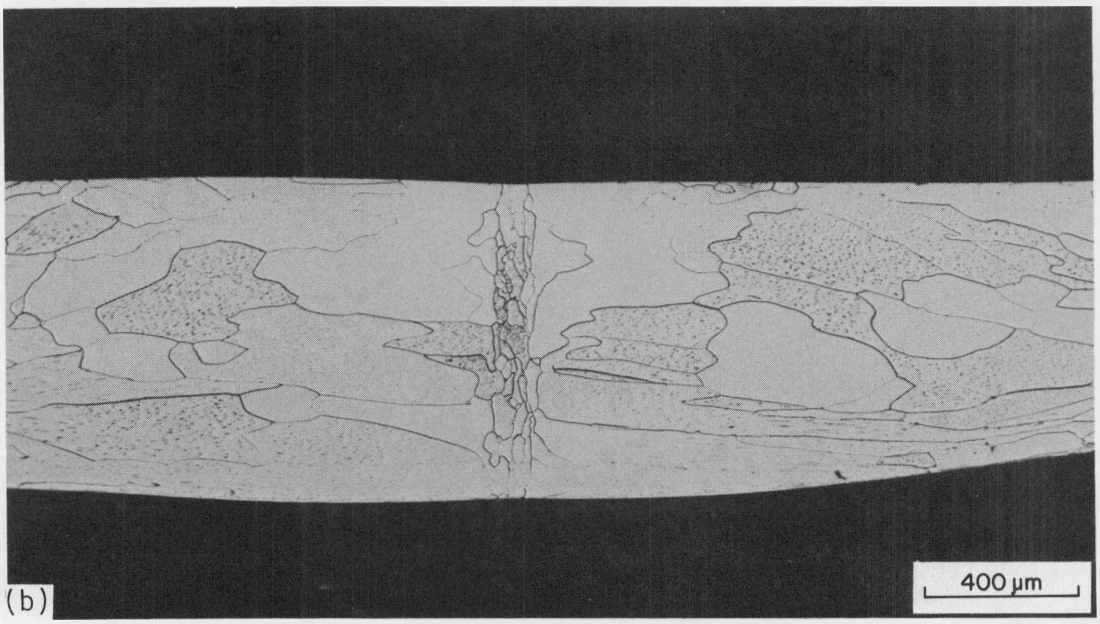

Fig. 4. Fusion zone microstructure of a DOP-26 weld with a wide-bead (3.7-mm) width; no postweld heat treatment. (a) Top surface. (b) Transverse section.

Y-171440

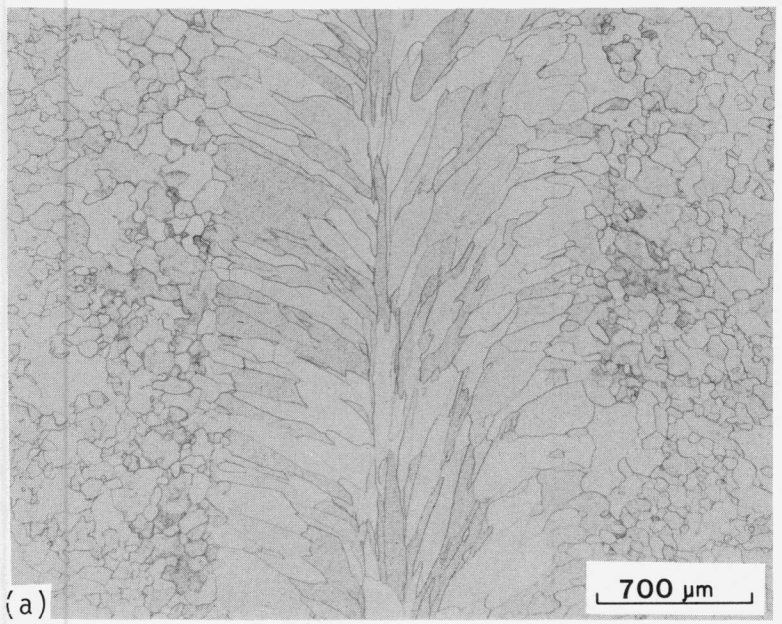

(a)

Y-171436

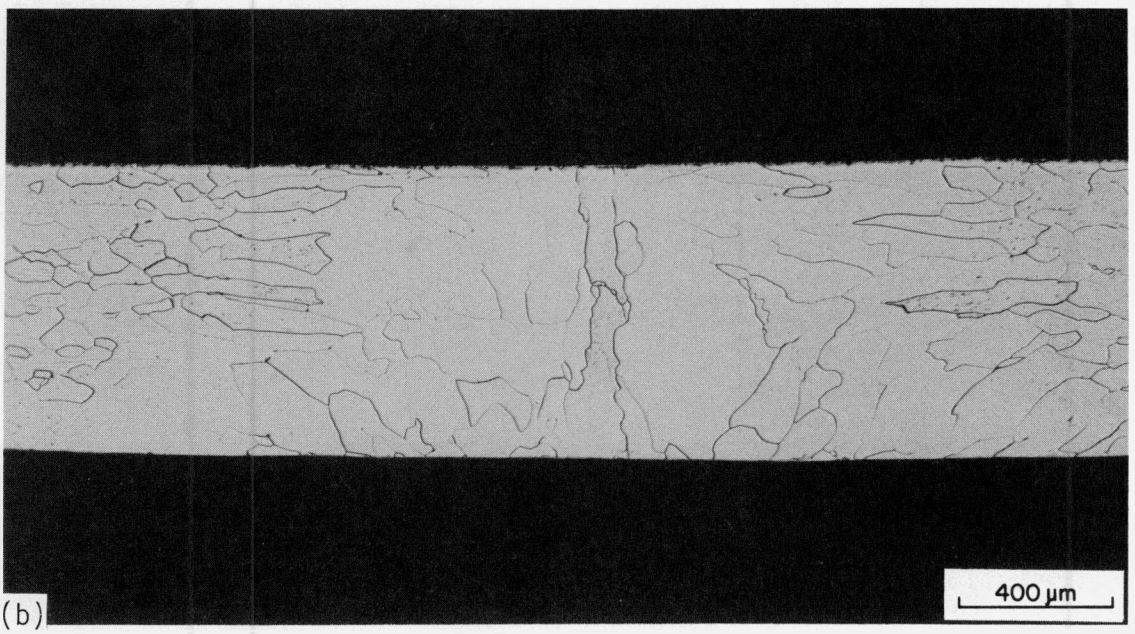

(b)

Fig. 5. Fusion zone microstructure of a DOP-26 weld with the narrow-bead width; postweld heat treatment: 1 h at 1500°C. (a) Top surface. (b) Transverse section.

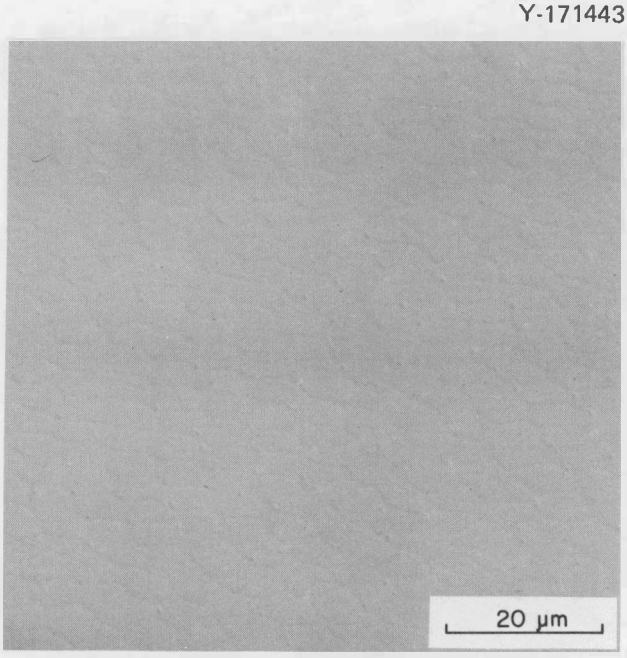

Fig. 6. Cellular dendritic structure within a grain of the fusion region of a DOP-26 narrow-bead weld.

Table 2. Tensile properties of DOP-26[a] gas tungsten arc welds tested at 650°C at a crosshead speed of 25 mm/min

Bead width[b]	Weld type	Postweld heat treatment		Weld-Test orientation[c]	Elongation (%)	Strength (MPa)	
		(h)	(°C)			Yield	Tensile
Wide	BOP[d]	None		Transverse	2.0	169.5	211.5
Wide	Butt	None		Transverse	3.1	164.7	291.5
Wide	Butt	1	1500	Transverse	4.3	119.9	275.6
Narrow	Butt	None		Transverse	10.5	173.6	508.5
Narrow	Butt	1	1500	Transverse	14.3	137.8	545.0
Narrow	Butt	1	1500	Longitudinal	21.5	164.7	462.3
Base metal			[e]		31.2	85.4	530.5

[a]DOP-26 annealed 1 h at 1500°C before welding.

[b]Wide, 3.7 ± 0.2 mm; narrow, 2.5 ± 0.2 mm.

[c]Transverse: specimens with a weld perpendicular to the tensile direction. Longitudinal: specimens with a weld parallel to the tensile direction.

[d]Bead-on-plate welds.

[e]Specimens annealed 1 h at 1500°C before testing.

1 h at 1500°C. The tensile properties of the narrow-bead weld were determined at directions both longitudinal and transverse to the weld as indicated in Table 2. The longitudinal weld specimen had an elongation of 21.5% and the transverse weld specimen had 14.3%.

The specimens with a transverse weld always fractured near the centerline of the fusion zone. The fracture surface was examined by SEM to identify the fracture mode. Figure 7 compares the fracture mode of the

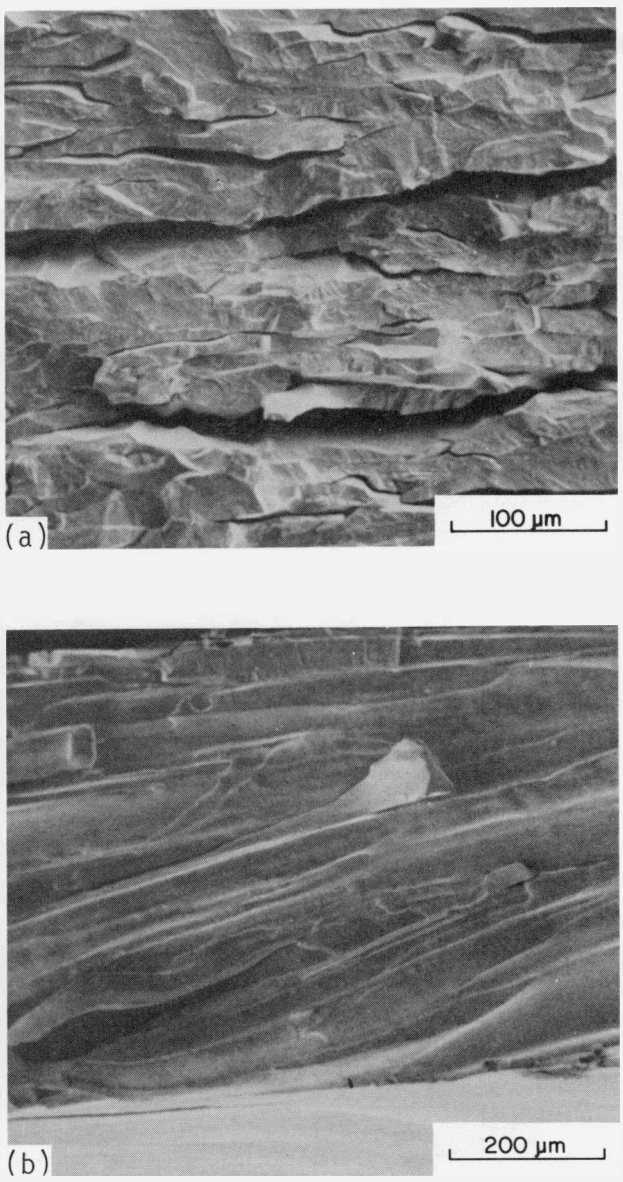

Fig. 7. Scanning electron microscopic fractographs of DOP-26 specimens tensile fractured at 650°C at a crosshead speed of 25 mm/min. (a) The base metal. (b) The transverse weld with the narrow-bead width (postweld heat treatment, 1 h at 1500°C).

base metal and the transverse weld with a narrow-bead width. The welded specimen showed grain boundary fracture with a very brittle appearance, whereas the base metal exhibited transgranular fracture with a high degree of secondary cracking. The grains appearing on the fracture surface are well elongated along the welding direction. In addition, their grain boundaries are smooth, clean, and free of extensive precipitation (e.g. eutectic structure). Figure 8(a) is a fractograph of the specimen with a longitudinal narrow weld. In this case, the fracture occurred

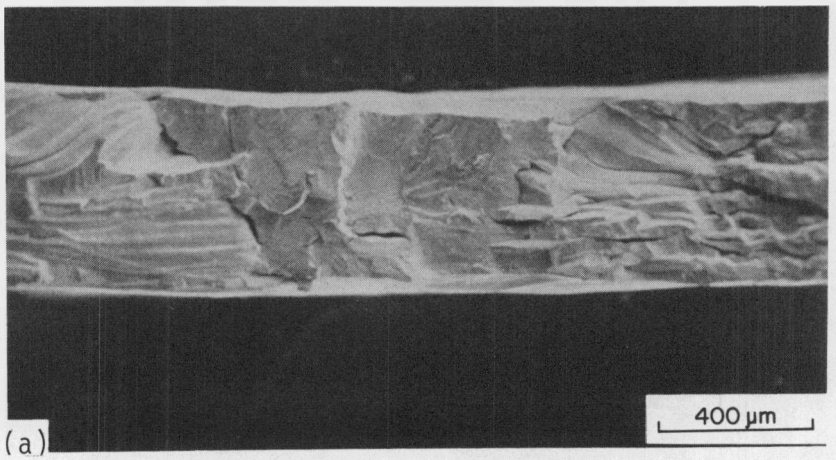

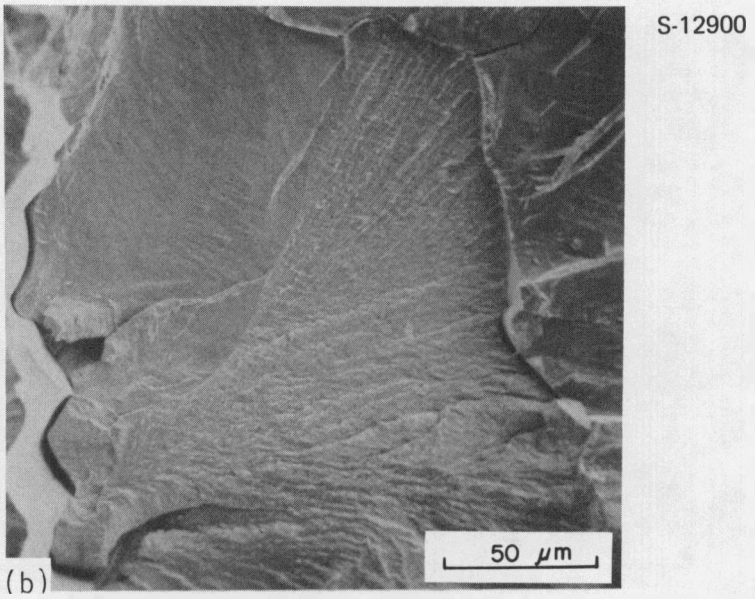

Fig. 8. Scanning electron microscopic fractograph of the DOP-26 specimen with a narrow longitudinal weld tensile fractured at 650°C. Postweld heat treatment, 1 h at 1500°C. (a) Fracture surface across the weld. (b) Transgranular cleavage in the center of the fusion zone.

across the weld with a duplex fracture mode, that is, a transgranular fracture in the central part of the fusion zone flanked by intergranular fracture in the outer region. The features of the transgranular cleavage can easily be identified at a high magnification [Fig. 8(b)]. Outside the fusion zone is the base metal, which was also fractured by transgranular cleavage at 650°C.

Impact Properties

Impact properties of DOP-26 GTA welds were determined from 800 to 1150°C at an impact velocity of 61 m/s (200 fps). Table 3 shows the effect of weld bead width and postweld heat treatment on impact properties of DOP-26 transverse weld specimens. The impact ductility of the narrow weld is much better than that of the wide weld. In fact, the impact elongation at 980 and 1100°C more than doubles as the surface bead width is reduced from 3.7 to 2.5 mm. The specimens exhibited low impact ductility in the as-welded condition, and a postweld heat treatment of 1 h at 1500°C produced a sharp increase in ductility for both wide and narrow welds. As indicated in Table 3, the impact ductility appears to be unaffected by the type of weld, butt or autogeneous bead-on-plate.

The impact properties of the DOP-26 welds heat treated for 1 h at 1500°C were characterized at directions both longitudinal and transverse to the welds. The impact data together with those of the base metal[15] are plotted as a function of test temperature in Fig. 9. The impact ductility of the base metal is much superior to that of the welds. The impact elongation of the welded specimens increases with test temperature, and the increase becomes more pronounced for the narrow weld above 980°C and for the wide weld above 1050°C. The transverse weld specimen with the wide-bead width has the lowest impact elongation, and the longitudinal weld specimen with the narrow-bead width has the highest elongation at all the test temperatures. The impact ductility of the transverse weld specimen with the narrow-bead width falls between the limits. At 1050°C the impact ductility is 4.0, 13.7, and 20.1 for the specimens with wide transverse, narrow transverse, and narrow longitudinal welds, respectively. Thus, the impact ductility of the DOP-26 welds is sensitive to both the bead width and the weld-test orientation.

Table 3. Effect of weld bead width and postweld heat treatment on impact properties of DOP-26 specimens[a] with a transverse weld (impact velocity: 61 m/s)

Weld condition		Impact temperature (°C)	Impact elongation (%)	
Bead width[b]	Type of weld		As-welded	Heat-treated[c]
Wide	Bead-on-plate	980	0.8	2.9
Wide	Butt	980		3.8
Narrow	Butt	980	3.4	8.3
Wide	Bead-on-plate	1100	4.2	6.5
Wide	Butt	1100		6.1
Narrow	Butt	1100	8.5	16.7

[a]DOP-26 specimens annealed 1 h at 1500°C before welding.

[b]Wide, 3.7 ± 0.2 mm; narrow, 2.5 ± 0.2 mm.

[c]Heat treated 1 h at 1500°C after welding.

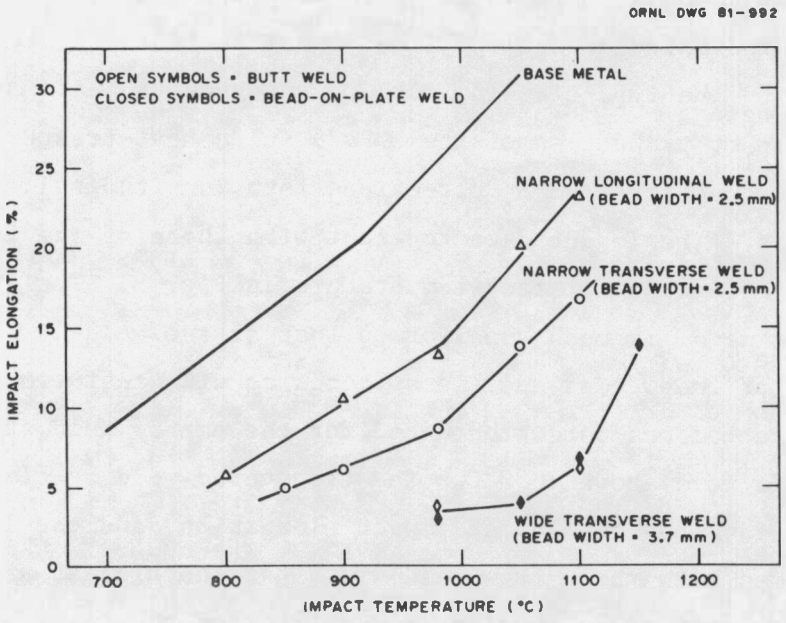

Fig. 9. Plot of impact elongation as a function of impact temperature for DOP-26 base metal and welds; impact velocity, 61 m/s; postweld heat treatment, 1 h at 1500°C.

The effect of postweld heat treatment on impact ductility is further demonstrated in Table 4 and Fig. 10. The ductility of the specimens with a transverse narrow weld increases with heat treatment and appears to reach a plateau after 100 h at 1260°C or 1 h at 1500°C (Table 4). With severe heat treatment such as 1 h at 1650°C plus 2 min at 1800°C, the weld exhibited a lower ductility (Fig. 10). The base metal also showed a marked drop in impact ductility after a long-term (4300-h) aging at 1300°C.

The impact fracture of the transverse weld specimens also occurred near the centerline of the fusion zone. Figure 11 shows SEM fractographs of the wide- and narrow-bead welds tested at 1100°C and 61 m/s. Both specimens exhibited brittle grain boundary fracture, and the grains in the wide-bead weld were elongated and parallel to the welding direction. The longitudinal weld specimens exhibited a duplex fracture (Fig. 12) similar to the tensile fracture at 650°C (Fig. 8). In the central region of the fusion zone, the fracture mode is mainly transgranular, with secondary tearing along grain boundaries that are essentially parallel to the tensile axis. In the outer region, the fracture is dominantly grain boundary separation.

Scanning electron microscopy at high magnification showed that second-phase particles occurred on the fracture surface. Figure 13(a) is a fractograph showing the fine particles and pores (without particles) on grain boundary facets in the fusion zone of a narrow weld. (Stains from exposure of the fracture surface to air for six months before examination are also visible in Fig. 13.) We identified the composition of the particles by energy dispersive x-ray analysis. The x-ray fluorescence spectra* from the regions with and without particles are compared in Fig. 13(b) and (c), respectively. A small Th $M\alpha$ peak at about 3 keV is observed in Fig. 13(b) but not in Fig. 13(c), which indicates the enrichment of thorium in the particle. Occasionally, an extensive precipitate occurred on the fracture surface of a wide-bead weld (Fig. 14). The precipitates are well aligned with a morphology somewhat similar to a eutectic patch.[12,14]

*A small Al $M\alpha$ peak at about 0.15 keV is observed in Fig. 13(b) and (c), most probably from the use of aluminum substrate.

Table 4. Effect of postweld heat treatment on impact properties of DOP-26 specimens[a] with a narrow transverse butt weld (test condition 980°C and 61 m/s)

Postweld heat treatment		Impact ductility (%)
Temperature (°C)	Time (h)	
None		3.1
None		3.4
1260	50	7.2
1260	100	8.6
1500	1	8.3

[a]Specimens annealed for 1 h at 1500°C before welding.

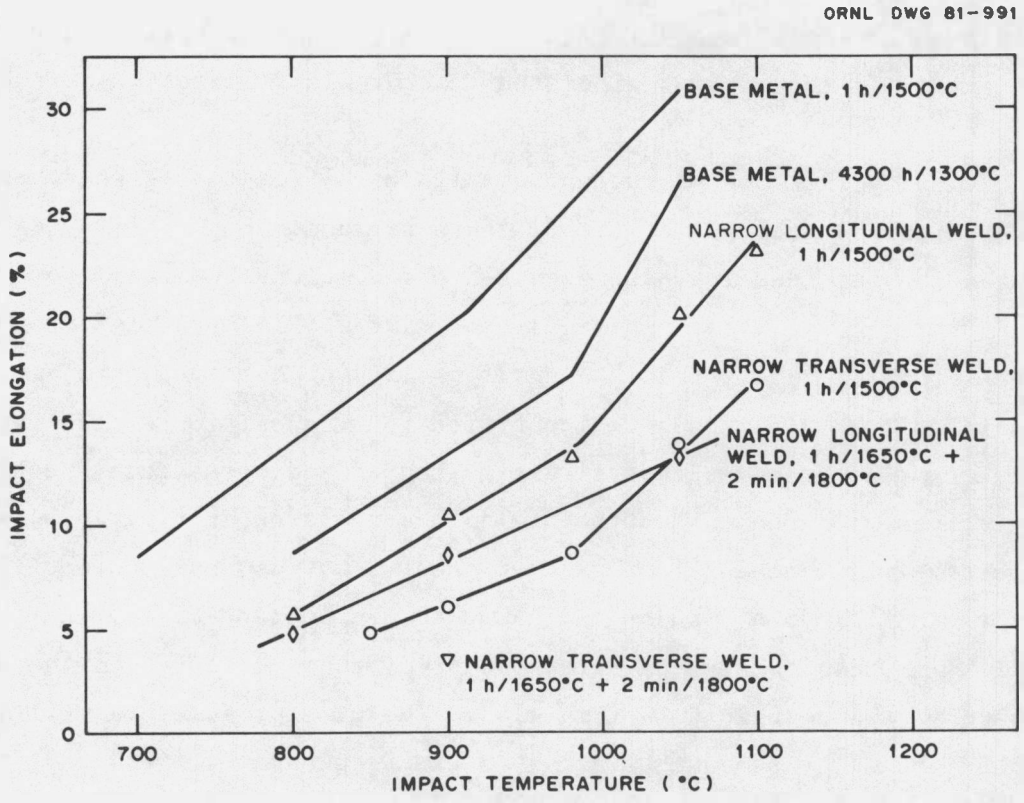

Fig. 10. Effect of postweld heat treatment and impact temperature on impact ductility of DOP-26 base metal and narrow weld; impact velocity 61 m/s.

S-12906

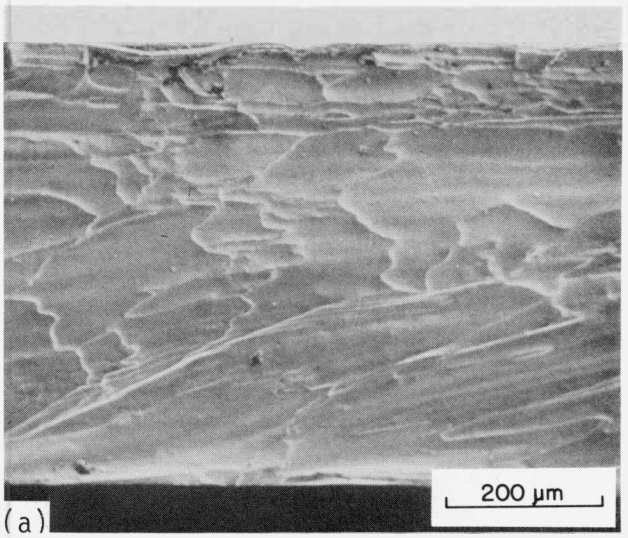

S-12193

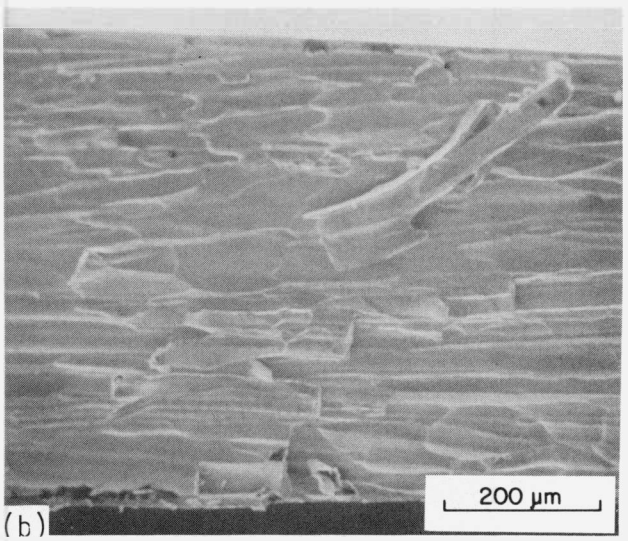

Fig. 11. Scanning electron microscopic fractographs of DOP-26 weld specimens impact fractured at 1100°C and 61 m/s; postweld heat treatment, 1 h at 1500°C. (a) Narrow-bead weld. (b) Wide-bead weld.

S-12216

Fig. 12. Scanning electron microscopic fractograph of the DOP-26 specimen with a narrow longitudinal weld impact-fractured at 900°C and 61 m/s; postweld heat treatment: 1 h at 1500°C.

ORNL-PHOTO 2016-82

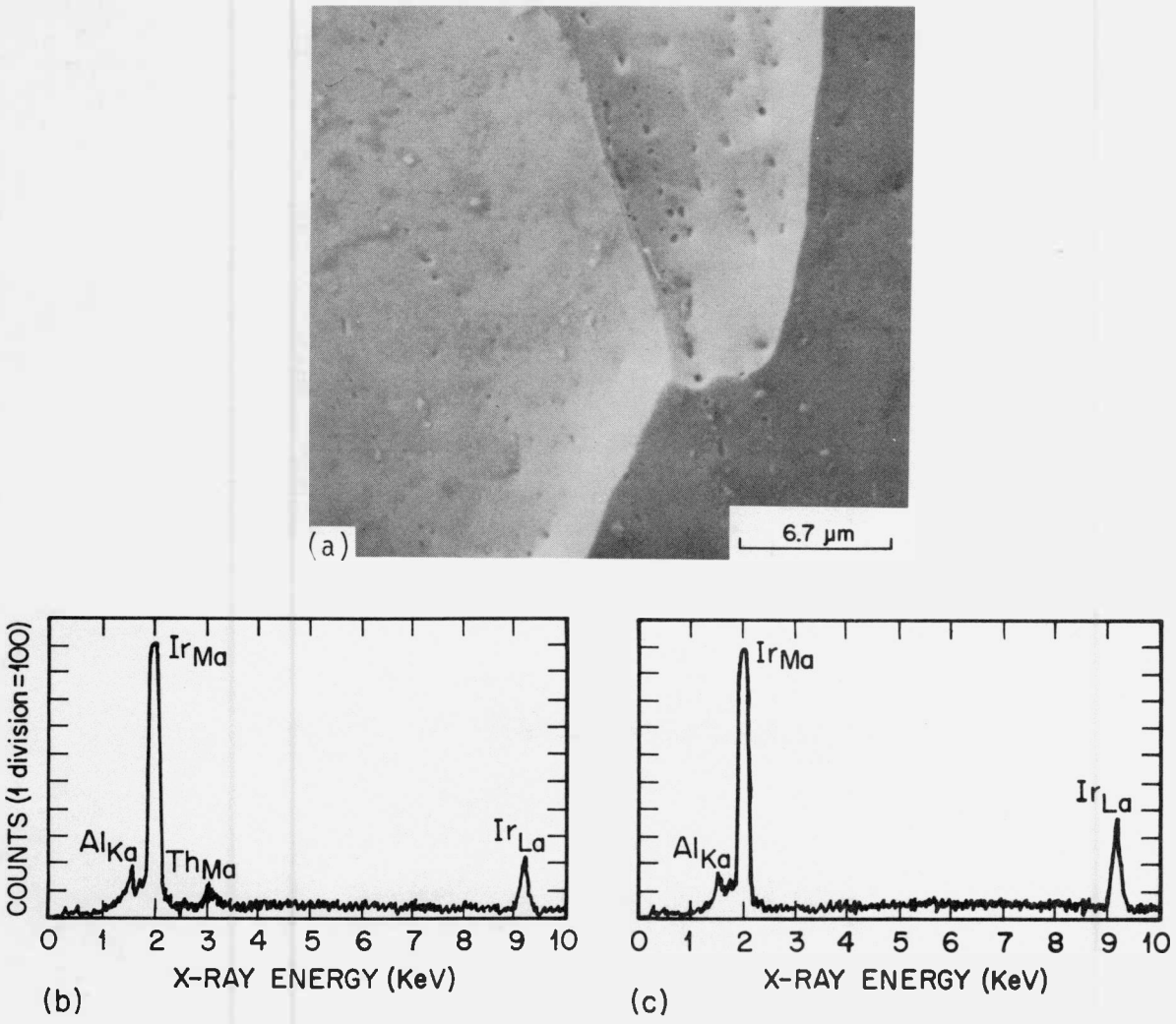

Fig. 13. (a) Scanning electron microscopic fractograph showing particles on grain boundary facets in the fusion zone of a narrow weld impact fractured at 1100°C and 61 m/s; postweld heat treatment, 1 h at 1500°C. (b) X-ray fluorescence spectrum from the region with a particle. (c) X-ray fluorescence spectrum from the region without particles.

9022

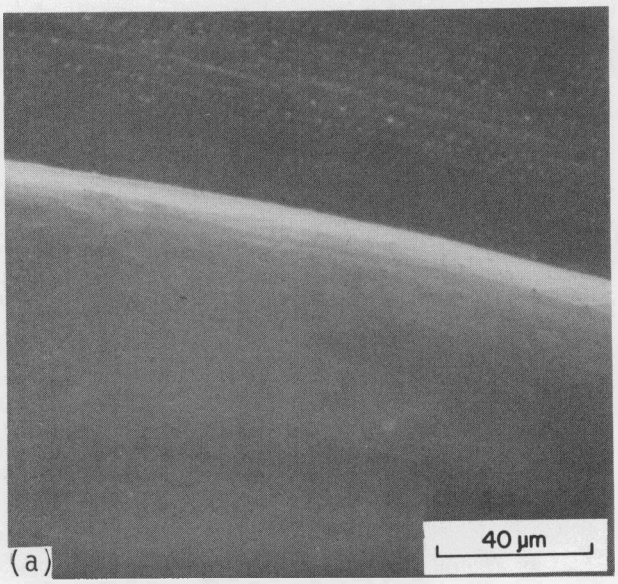

9023

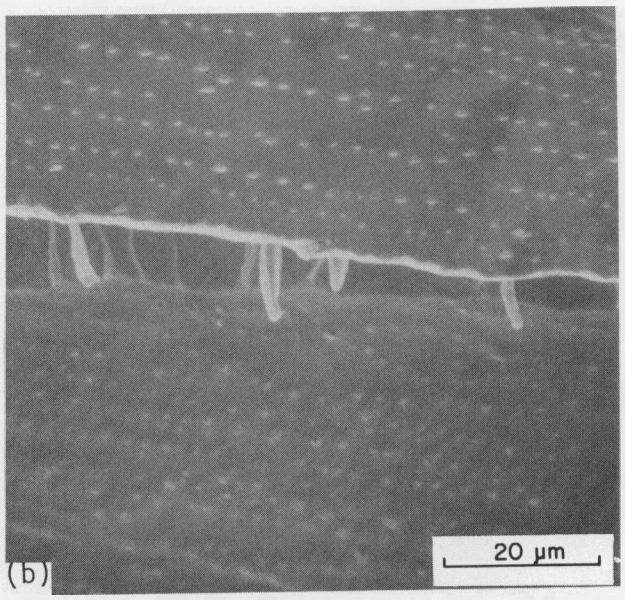

Fig. 14. Scanning electron microscopic fractographs showing well-arrayed particles on the fracture surface of the wide-bead (3.7-mm) weld.

DISCUSSION

The fusion zone grain structure is known to be governed by the weld puddle shape.[14] The difference in weld structure in the wide- and narrow-bead welds can be explained on the basis of change in weld puddle shape with bead width or heat input. Figure 15 is a sketch of the two-dimensional shape of the weld puddles and their associated fusion zone grain structures. The trailing edge of the wide-bead weld puddle gets drawn out so that the puddle appears to be teardrop shaped. The grains in the fusion zone of the wide weld nucleate on the partially melted base metal grains and continue to grow normal to the solid-liquid interface. The teardrop-shaped puddle provides almost an invariant direction of maximum thermal gradient at all points on the pool edge from the fusion boundary almost to the weld centerline. This results in development of columnar grains toward the centerline of the weld. Since some favorably oriented grains grow at the expense of unfavorably oriented grains, this leads to development of a coarse columnar grain structure toward the weld centerline. This growth of the columnar grains toward the centerline was eventually interrupted by a band of grains growing parallel to the welding direction as a result of the teardrop-shaped weld puddle [Fig. 15(a)].

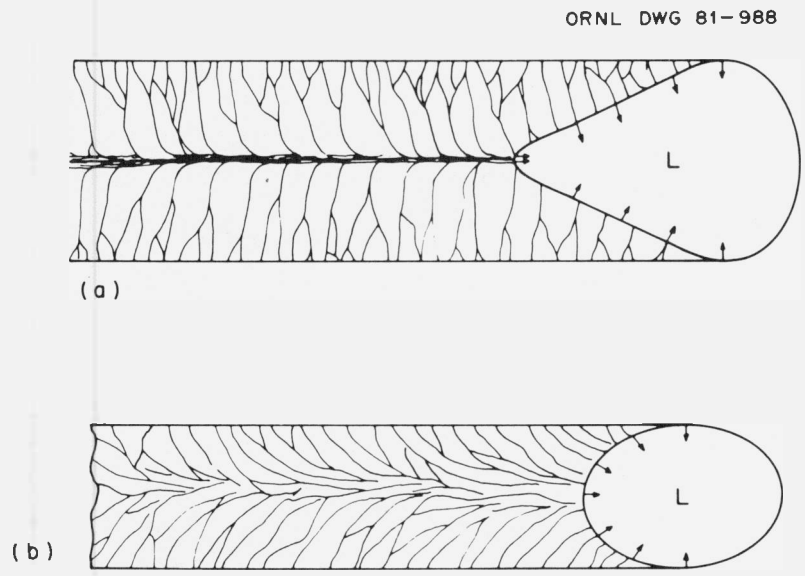

Fig. 15. Fusion zone structure development in (a) wide-bead (3.7-mm) weld with a teardrop shaped weld puddle and (b) narrow-bead (2.5-mm) weld with an elliptical weld puddle.

With low heat input, the puddle assumes an elliptical shape [Fig. 15(b)] and the weld bead for the same welding speed is narrower. The direction of maximum thermal gradient on the elliptical puddle changes continuously from the fusion boundary to the weld centerline. Consequently, no single grain experiences favored growth direction for an extended period, and many grains from the fusion line survive to reach the centerline of the weld. This results in the growth of grains that exhibit considerable curvature [Figs. 15(b) and 3(a)] and also leads to a relatively finer fusion zone structure for the narrow-bead weld. However, for a given bead width, the puddle shape can be altered by a proper selection of welding parameters such as current and welding speed. A detailed discussion of this has been presented elsewhere.[14]

In addition to the grain structure, bead width and heat input also influence the segregation of thorium and the precipitation of a thorium-rich phase along grain boundaries. Previous studies[12,14] indicated that the alloys containing more than 100 ppm Th were prone to hot cracking during GTA welding. Weld metal cracking is identified as the combined effects of liquation cracking in the HAZ and solidification cracking along the centerline of welds. Scanning electron microscopic examination of fracture surfaces revealed patches of low-melting eutectic in the alloy doped with 200 ppm Th. The susceptibility of hot cracking was found to decrease with decreasing heat input. Successful welds without hot cracking had been obtained in the 200 ppm Th alloy by use of highly concentrated heat sources, such as laser beam[14] and electron beam.[12] In contrast to the 200 ppm Th alloy, hot cracking does not occur during GTA welding of the DOP-26 alloy containing 60 ppm Th. Nevertheless, patches of well-arrayed precipitates (Fig. 14) occur on the fracture surface of the wide-bead weld. Energy dispersive analysis indicates that the precipitates are enriched in thorium, probably Ir_5Th. The formation of eutectic-like precipitates in the wide-bead welds is believed to result from a larger fused volume and a slower cooling rate (as compared with the narrow-bead weld), both of which enhance the segregation of thorium during later stages of precipitation.

Tensile and impact tests indicate that the ductility and fracture behavior of the DOP-26 alloy are sensitive to weld bead width, postweld

heat treatment, and weld-test orientation. All these parameters affect the fusion zone grain structure and fracture path of the welds. Mechanical properties of iridium, like refractory metals and alloys, depend strongly on its microstructure.[6,8,10,11] The grain boundaries in iridium and Ir—0.3% W alloys are intrinsically weak and tend to be preferred sites for nucleation and propagation of cracks. The brittle fracture associated with grain boundary separation is always promoted in iridium materials by an increase in grain size or strain rate or by a decrease in test temperature. All these results can be rationalized[8,11] on the basis of stress concentration at the grain boundaries. For example, the coarser the grain size, the higher the stress concentration that initiates cracks along the grain boundaries at an early stage of deformation, thereby lowering the overall ductility of iridium alloys. To improve the ductility and fracture behavior, Ir—0.3% W alloy was doped with 30 to 200 ppm Th (refs. 10 and 11). The tensile tests at 650°C revealed that the thorium-doped alloys failed mainly by transgranular fracture rather than by grain boundary separation. Also, the doped alloys showed ductile rupture with substantial reduction of area in impact tests at temperatures above 1000°C. Auger analysis on the fractured surface indicated a preferential segregation of thorium to iridium grain boundaries. It is therefore believed that the suppression of grain boundary fracture in the doped alloys is caused by the strong segregation of thorium to iridium grain boundaries, which apparently improves the mechanical properties of the boundaries. Also an analysis of the impact data from a dislocation pileup model indicates that an enrichment of 5 to 10% Th at iridium grain boundaries increases the cohesive strength of the boundary by 90%.[11]

The DOP-26 welds exhibit tensile and impact ductility distinctly lower than those of the base metal. The lower ductility of the welded specimens is mainly due to the coarser grain structure in the fusion zone (Figs. 3—5). As mentioned in the foregoing section, the ductility of Ir—0.3% W alloys decreases, and the propensity for grain boundary fracture increases with increasing grain size. The coarse grain structure in the fusion zone induces a high stress concentration at grain boundaries during plastic deformation, thereby promoting the brittle grain boundary fracture

and thus lowering the overall ductility of the welded specimens. The grain size effect is further evidenced in Fig. 10 by comparing the impact elongation of specimens heat treated for 1 h at 1500°C and specimens for 1 h at 1650°C plus 2 min at 1800°C. The severe duplex heat treatment lowers the ductility of the welds because of excessive grain growth. A similar reduction in weld ductility has been observed in other metals such as tantalum[16] and molybdenum.[17]

Tables 2 and 3 and Figs. 9 and 10 show that the ductility of DOP-26 welds depends on bead width and weld-test orientation. All the results can be rationalized from consideration of fusion zone grain structure and fracture path of the welded specimens.[16,18] The specimens tested transverse to the welding direction [Fig. 1(a)] fractured along the centerline of the fusion zone, whereas the specimens pulled longitudinal to the welding direction (Fig. 16) failed across the welded region. Because the grains in the central part of the fusion zone are well elongated, the failure path for the longitudinal weld specimens must fracture these grains transgranularly. This is evidenced in Figs. 8 and 12, where transgranular fracture occurred at the central part of the fusion region and grain boundary fracture occurred in the outer region. Because more energy is dissipated for the transgranular fracture, the longitudinal weld specimens showed better ductility than did the transverse weld specimens, which exhibited 100% grain boundary fracture. Welds with the narrow-bead width are also much more ductile than are welds with wide-bead width. The lower ductility of the wide-bead weld is due to its unfavorable fusion zone grain structure [Fig. 15(a)]. As shown in Fig. 4, the weld with the wide-bead width showed a columnar grain structure in the outer region of the fusion zone and a narrow band of elongated grain structure along the centerline region. The directions of the grain boundaries in the fusion zone coincide with both the fracture paths for specimens pulled longitudinal and transverse to the welding direction, thereby promoting the brittle grain boundary fracture. Furthermore, the formation of well-arrayed precipitates with morphology similar to an eutectic structure is expected to further embrittle the grain boundaries and lower the ductility of the wide weld. The grain boundary embrittlement has been observed[11] in the base metal of Ir—0.3% W doped with 1000 ppm Th because of an excessive precipitation of $ThIr_5$ particles at the boundaries.

The above discussion suggests a possible correlation of ductility with the fracture behavior of the DOP-26 alloy. We illustrate the correlation in Fig. 16: the ductility of the base metal and welds is plotted as a function of the transgranular fracture. The elongations obtained from tensile tests at 650°C and impact tests at 900 and 1050°C are used in the plot. The transgranular fracture is estimated from SEM fractographs. The elongation of the base metal and welds increases with increasing transgranular fraction. In fact, a linear relationship is held for the data obtained at 650 and 900°C. These results strongly indicate that the low ductility of DOP-26 welds is due to the brittle grain boundary fracture from a combined effect of the coarse grain structure and unfavorable grain orientation in the fusion zone of the GTA welds.

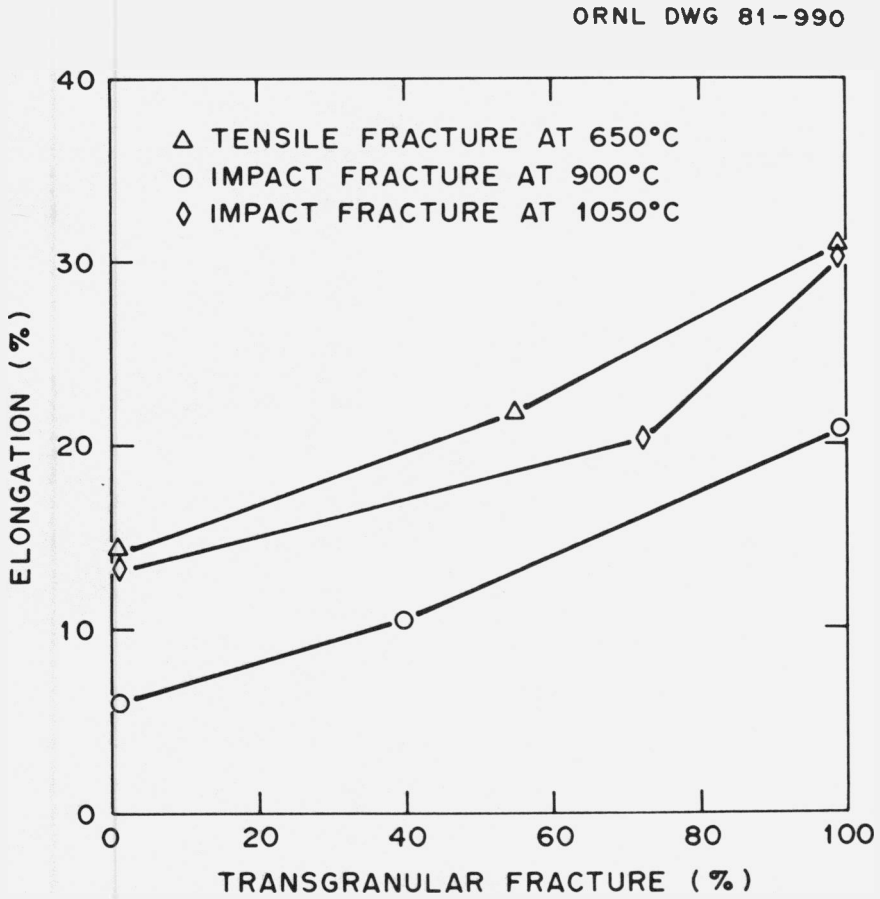

Fig. 16. Plot of tensile and impact elongation of DOP-26 base metal and welds as a function of percent of transgranular fracture.

The DOP-26 welds showed a significant increase in tensile and impact ductility after postweld heat treatments at 1300 and 1500°C. The increase in ductility of welds by proper heat treatment has also been observed in molybdenum and tantalum alloys.[16,17,19] Inasmuch as the heat treatments do not significantly change the grain structure of DOP-26 welds, the improvement in ductility may come from a reduction in thermal and shrinkage stresses generated during GTA welding. To verify this, microhardness measurements were made on DOP-26 welds with and without a postweld heat treatment of 1 h at 1500°C. As shown in Table 5, the heat treatment causes a drop in microhardness in both the fusion and heat-affected zones, most probably from the stress-relief effect.

Table 5. Microhardness of DOP-26 gas tungsten arc welds[a]

Weld bead width[b]	Postweld heat treatment	Fusion region (DPH)		Heat-affected zone (DPH)
		Center	Outer	
Wide	None	260	251	273
Wide	1 h/1500°C	232	231	238
Narrow	None	254	251	250
Narrow	1 h/1500°C	234	234	235

[a]Specimens were annealed 1 h at 1500°C before welding.

[b]Wide, 3.7 ± 0.2 mm; narrow, 2.5 ± 0.2 mm.

SUMMARY AND CONCLUSIONS

Weld metal grain structure and mechanical properties of the Ir–0.3% W alloy (DOP-26) doped with 60 ppm Th and 50 ppm Al have been investigated. Butt and autogeneous bead-on-plate welds were performed on 0.64-mm sheets with the GTA process. The fusion zone grain structure depends strongly on heat input and puddle shape and therefore on the bead width. The grains in the fusion zone of a narrow-bead (2.5-mm) weld are fine and appear to nucleate on the partially melted base metal grains and to grow continuously, with most of the grains exhibiting a considerable curvature.

In comparison, the grains in a wide-bead (3.7-mm) width weld grow almost normal to the welding direction until reaching the centerline region. Along the centerline region, the grains show a sharp change in growth direction and develop a fine columnar structure with grains growing parallel to the welding direction. The difference in weld fusion zone structure is the result of a change in weld puddle from an elliptical shape for the narrow weld to a teardrop shape for the wide weld.

Mechanical properties of the welds and base metal were characterized by tensile and impact tests from 650 to 1150°C. The ductility and fracture behavior of DOP-26 welds are sensitive to weld bead width, postweld heat treatment, and weld-test orientation. The tensile ductility of the welds at 650°C is significantly higher for the narrow-bead weld than for the wide-bead weld. Both types of welds show a remarkable increase in ductility and decrease in yield strength after a postweld treatment of 1 h at 1500°C. The transverse weld specimens show grain boundary fracture with a very brittle appearance, whereas the base metal exhibited transgranular fracture with a high degree of secondary cracking. The fracture of the longitudinal weld specimens occurred across the weld with a duplex fracture mode, that is, a transgranular fracture in the central part of the fusion zone flanked by intergranular fracture in the outer region. Because of the mixed fracture mode, the longitudinal weld specimens show better ductility than do the transverse weld specimens.

The impact elongation of the welded specimens increases with test temperature, and the increase becomes more pronounced for the narrow weld at temperatures above 980°C and for the wide-bead weld above 1050°C. The transverse weld specimen with the wide bead has the lowest impact ductility at all the test temperatures, and the longitudinal weld with the narrow-bead width has the highest elongation. The impact ductility of the transverse weld specimen with the narrow-bead width falls between the limits. All these results can be rationalized from consideration of fusion zone grain structure and fracture path. The lower ductility of the wide-bead weld is mainly due to its unfavorable fusion zone grain structure, which has a columnar grain structure in the outer region and a narrow band of elongated grain structure along the centerline region. The

directions of the grain boundaries in the fusion zone coincide with both the fracture paths for specimens pulled longitudinal and transverse to the welding direction, thereby promoting the brittle grain boundary fracture.

The DOP-26 specimens exhibited low impact ductility in the as-welded condition. However, postweld heat treatments at 1500 and 1300°C produced a sharp increase in ductility for both the wide and narrow welds. Microhardness measurements suggest that the improvement in ductility is a result of a reduction in thermal and shrinkage stresses generated during GTA welding. With a severe heat treatment (such as 1 h at 1650°C plus 2 min at 1800°C), the welds exhibited a lower ductility. The lowering in ductility is caused by an excessive grain growth during the heat treatment.

ACKNOWLEDGMENTS

The authors gratefully acknowledge the encouragement of C. O. Tarr of the Department of Energy and R. H. Cooper, Jr., program manager. The authors also acknowledge A. C. Schaffhauser, H. Inouye, C. L. White, and R. L. Heestand for valuable discussions. Thanks are due to F. L. Ball for scanning electron microscopy, E. H. Lee and J. F. Newsome for technical assistance, C. P. Halton for metallography, and J. D. Hudson for GTA welding. Finally we acknowledge Irene Brogden for editing and P. T. Thornton for preparing the manuscript for publication.

REFERENCES

1. W. Koster, *Appl. Sci. Res.*, 4, 329–35 (1953–54).

2. P. Haasen, H. Hicker, and B. L. Mordike, *Z. Metallkd.* 56, 832–41 (1965).

3. R. W. Douglass and R. I. Jaffee, "High-Temperature Properties and Alloying Behavior of the Refractory Platium-Group Metals," *Proc. Am. Soc. Test. Mater.* 62, 627–37 (1962).

4. C. A. Brookes, J. H. Greenwood, and J. L. Routbort, "The High-Temperature Tensile Properties of Iridium Single Crystals," *J. Inst. Met.* 98, 27–31 (1970).

5. A. S. Tetelman and A. J. McEvily, Jr., *Fracture of Structural Materials*, John Wiley, New York, 1967, p. 212.

6. C. T. Liu and H. Inouye, *Study of Iridium and Iridium-Tungsten Alloys for Space Radioisotopic Heat Sources*, ORNL-5240, December 1976.

7. S. S. Hecker, D. L. Rohr, and D. F. Stein, "Brittle Fracture in Iridium," *Metall. Trans. A* 9A, 481–87 (1978).

8. C. T. Liu and H. Inouye, "Effect of Impurity, Grain Size, Test Temperature, and Grain Size on Fracture Behavior of Ir and Ir–0.3% W Alloys," pp. 1149–53 in *Proc. 2d Int. Conf. Mech. Behav. Mater., Boston, Aug. 16–20, 1976*, American Society for Metals, Metals Park, Ohio, 1976.

9. C. L. White, R. E. Clausing, and L. Heatherly, "The Effect of Trace Element Additions on the Grain Boundary Composition of Ir + 0.3% W Alloys," *Metall. Trans. A* 10A, 683–91 (1979).

10. C. T. Liu and H. Inouye, *Development and Characterization of an Improved Ir–0.3% W Alloy for Space Radioisotopic Heat Sources*, ORNL-5290, October 1977.

11. C. T. Liu, H. Inouye, and A. C. Schaffhauser, "Effect of Thorium Additions on Metallurgical and Mechanical Properties of Ir–0.3% W Alloys," *Metall. Trans. A* 12A, 993–1002 (1981).

12. S. A. David and C. T. Liu, "Weldability and Hot Cracking in Thorium-Doped Iridium Alloys," *Met. Technol. (N.Y.)* 7, 102–06 (1980).

13. D. L. Coffey, N. H. Jones, W. B. Artnmill, and W. A. Saul, "Parametric Modification of Weld Microstructure in Iridium," *Weld. J. (Miami, Fla.)* 53, 566–68 (1974).

14. S. A. David and C. T. Liu, *High-Power Laser and Arc Welding of Th-Doped Ir Alloys*, ORNL/TM-7258, May 1980.

15. C. T. Liu, unpublished data.

16. P. A. Kammer, R. E. Monroe, and D. C. Martin, "Weldability of Tantalum Alloys," *Weld. J. (Miami, Fla.)* 51, 304–19 (1972).

17. G. N. Alekseenko, S. M. Gurenich, and M. M. Nersdenko, "Weldability of the TSM-4 Molybdenum Alloy," *Avtom. Svarka* 26(5), 45–48 (1973).

18. Y. Sharin, J. Pelleg, and A. Grill, "Effect of Arc Vibration and Current Pulse on Microstructure and Mechanical Properties of TIG Tantalum Welds," *Met. Technol. (N.Y.)* 5, 190–96 (1978).

19. G. N. Alekseenko, M. M. Nerodeko, V. A. Lizunov, V. N. Minakov, and V. T. Trefilov, "Analysis of the Conditions for the Breakdown of Welds in Molybdenum Alloys," *Avtom. Svarka* 28(1) 58–60 (1975).

ORNL-5857
Distribution
Category UC-23

INTERNAL DISTRIBUTION

1–2. Central Research Library
3. Document Reference Section
4–5. Laboratory Records Department
6. Laboratory Records, ORNL RC
7. ORNL Patent Section
8. P. Angelini
9. R. H. Cooper, Jr.
10. R. S. Crouse
11–15. S. A. David
16. G. M. Goodwin
17. R. L. Heestand
18–20. M. R. Hill
21. H. Inouye
22. J. S. Ivey
23. J. R. Keiser
24. C. C. Koch
25–29. C. T. Liu
30. M. M. Martin
31. G. M. Slaughter
32. J. O. Stiegler
33. V. J. Tennery
34. C. L. White
35. F. W. Wiffen
36. A. L. Bement, Jr. (Consultant)
37. E. H. Kottcamp, Jr. (Consultant)
38. Alan Lawley (Consultant)
39. T. B. Massalski (Consultant)
40. R. H. Redwine (Consultant)
41. K. M. Zwilsky (Consultant)

EXTERNAL DISTRIBUTION

42. AIR FORCE WEAPONS LABORATORY, Kirtland Air Force Base, DYUS, Albuquerque, NM 87116

Michael Seaton

43–44. BATTELLE COLUMBUS LABORATORIES, 505 King Ave., Columbus, OH 43201

E. L. Foster
I. M. Grinberg

45–46. E. I. du Pont de Neumors, SAVANNAH RIVER LABORATORY, Aiken SC 29801

R. T. Huntoon
R. H. Tait

47–48. E. I. du Pont de Nemours, SAVANNAH RIVER PLANT, Aiken, SC 29801

R. A. Brownback
W. R. Kanne

49–51. FAIRCHILD INDUSTRIES, 20301, Century Blvd., Germantown, MD 20767

M. Eck
H. P. Kling
A. Schock

52. GENERAL ATOMIC CO., P.O. Box 81608, San Diego, CA 92138

N. B. Elsner

53–55. GENERAL ELECTRIC CO., Valley Forge Space Center, P.O. Box 8048, Philadelphia, PA 19101

V. Haley
R. J. Hemler
C. W. Whitmore

56–59. JET PROPULSION LABORATORY, California Institute of Technology, 4800 Oak Grove Drive, Pasadena, CA 91103

R. W. Campbell
J. E. Mondt
R. J. Spehalski
A. E. Wolfe

60. JOHNS HOPKINS UNIVERSITY, Applied Physics Laboratory, Johns Hopkins Road, Laurel, MD 20810

J. C. Hagan

61–62. LOS ALAMOS SCIENTIFIC LABORATORY, P.O. Box 1663, Los Alamos, NM 87545

R. D. Baker
S. E. Bronisz

63–66. MINNESOTA MINING AND MANUFACTURING CO., St. Paul, MN 55101

R. B. Ericson
E. F. Hampl
J. D. Hinderman
W. C. Mitchell

67–68. MONSANTO RESEARCH CORP., P.O. Box 32, Miamisburg, OH 45342

W. R. Amos
E. W. Johnson

69. SUNDSTRAND ENERGY SYSTEMS, 4747 Harrison Ave., Rockford, IL 61101

E. Krueger

70–71. TELEDYNE ENERGY SYSTEMS, 110 W. Timonium Rd., Timonium, MD 21093

W. J. Barnett
W. E. Osmeyer

72–82. DOE, DIVISION OF ADVANCED NUCLEAR SYSTEMS AND PROJECTS, Washington, DC 20545

G. L. Bennett
R. C. Brouns
F. M. Dieringer
J. S. Griffo
W. D. Kenney
J. J. Lombardo
R. B. Morrow
P. A. O'Riordan
W. C. Remini
B. J. Rock
C. O. Tarr

83–86. DOE, ALBUQUERQUE OPERATIONS OFFICE, P.O. Box 5400, Albuquerque, NM 87115

D. Foster
D. L. Krenz
D. K. Nowlin
D. Plymale

87. DOE, DAYTON AREA OFFICE, P.O. Box 66, Miamisburg, OH 45342

H. N. Hill

88. DOE, OAK RIDGE OPERATIONS OFFICE, P.O. Box E, Oak Ridge, TN 37830

J. A. Lenhard

89–90. DOE, SAN FRANCISCO OPERATIONS OFFICE, 1333 Broadway, Wells Fargo Building, Oakland, CA 94612

L. Lanni
W. L. Von Flue

91–92. DOE, SAVANNAH RIVER OPERATIONS OFFICE, P.O. Box A, Aiken, SC 29801

W. T. Goldston
W. D. Sandberg

93–229. Given distribution as shown in TIC-4500 under UC-23 category (Radioisotope and Radiation Applications - 25 copies for NTIS)

☆ U.S. GOVERNMENT PRINTING OFFICE 1982-546-067/103